

https://doi.org/10.1070/QEL17397

Decay of a laser beam under stimulated temperature scattering in toluene as a result of two-photon pump absorption and nonsteady-state laser pulse interaction with matter

A.A. Gordeev, V.F. Efimkov, I.G. Zubarev, S.I. Mikhailov

Abstract. **The decay of the pump-beam spatial structure under conditions of stimulated temperature scattering of a pulsed laser beam in toluene as a result of two-photon absorption of pump radiation and time-dependent interaction of a laser pulse with a medium is considered.**

Keywords: *stimulated temperature scattering, two-photon absorption of light in toluene, decay of a pump-beam spatial structure.*

In view of the development of efficient methods for fabricating dielectric and metal nanoparticles, many studies of various processes occurring in suspensions of these particles have been published in the last decade. In particular, He et al. [1–4] observed stimulated temperature scattering (STS) of light in such media, including suspensions of different metal nanoparticles in toluene [3]. It was shown in [5] that, at STS of the neodymium-laser second harmonic with a wavelength 0.53 μm in a suspension of silver nanoparticles in toluene, as well as in pure toluene, the spectral shift of the anti-Stokes component is almost an order of magnitude larger than the value given by the stationary scattering theory. The physical reason for this difference is the significant nonstationarity of the STS of short laser pulses [6], when their duration τ_{las} becomes comparable with the thermal-grating relaxation time $\tau_r = 1/(\chi q^2)$ (χ is the thermal diffusivity of the material and q is the modulus of the thermal-grating wave vector). At the same time, excellent agreement between experimental and theoretical results was observed under stationary conditions [7]. It should be noted here that the STS of the neodymium-laser second harmonic in pure toluene develops as a result of two-photon absorption at a wavelength of 0.53 μm [5, 6]. According to our estimates, the two-photon absorption coefficient is $(0.5–1)\times10^{-9}$ cm MW^{-1} in this case.

The emphasis in [5, 6] was on the spectral characteristics of the process. In continuation of those studies, we measured the time and energy parameters of interacting-wave pulses. Figure 1 shows typical oscillograms of the observed pulses. A noteworthy feature is their unusual temporal behaviour. The pulse of the anti-Stokes STS component ends prior to the pump pulse. But at the same time, as the pump pulse emerges from the active medium, the power of pump radiation continues to increase despite the presence of two-photon absorption. Our attempts to describe mathematically this temporal behaviour of pulses were unsuccessful. The most likely reason is that the plane-wave model used in the calculations is not appropriate for the process under study. Under our experimental conditions, the active medium in the focal-waist region is significantly heated, which leads to a pump-beam spatial transformation that cannot be described within the plane-wave model. To check this hypothesis, we measured the spatial structures of interacting waves in the focal-waist region when observing STS of the neodymium-laser second harmonic in toluene. The results of these measurements are discussed in this paper.

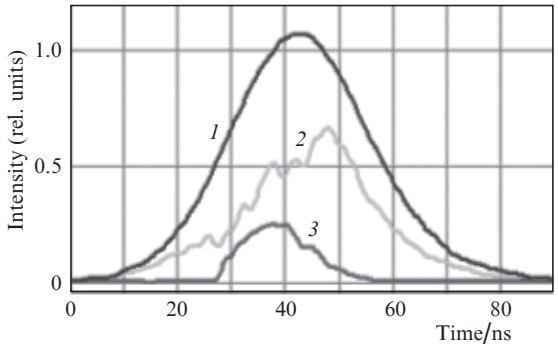

Figure 1. Oscillograms of interacting-wave pulses: (*1*, *2*) pump pulses at the (*1*) input and (*2*) output of the active medium and (*3*) backscattered-radiation pulse at STS.

Along with STS, stimulated Brillouin scattering (SBS) can also be observed in toluene. The conditions at which STS occurs in the absence of obscuring SBS were experimentally determined in [6]. The measurements described below were performed under these conditions.

A schematic of the experimental setup is presented in Fig. 2. The pump radiation in use was the second harmonic of a single-frequency single-mode neodymium laser. The duration of a pump pulse was about 30 ns, and the pump beam divergence was approximately 3×10^{-4} rad. The recording system made it possible to measure the energy and shape of pulses, as well as the divergences of all interacting beams. Photodiodes FD-7K with an integrating circuit served as calorimeters; their output pulses were fed to a Rigol DS 5062M storage oscilloscope with a transmission band of 60 MHz. The pulse shape was recorded using G6854-01 photodiodes with a transmission band of 2 GHz; their output pulses were fed to a GDS-73504A storage oscilloscope (GWINSTEK) with a transmission band of 500 MHz. The spatial structures

A.A. Gordeev, V.F. Efimkov, I.G. Zubarev, S.I. Mikhailov Lebedev Physical Institute, Russian Academy of Sciences, Leninsky prosp. 53, 119991 Moscow, Russia; e-mail: efimkovvf@lebedev.ru

Received 7 July 2020; revision received 3 September 2020
Kvantovaya Elektronika **50** (11) 1078–1082 (2020)
Translated by Yu.P. Sin'kov

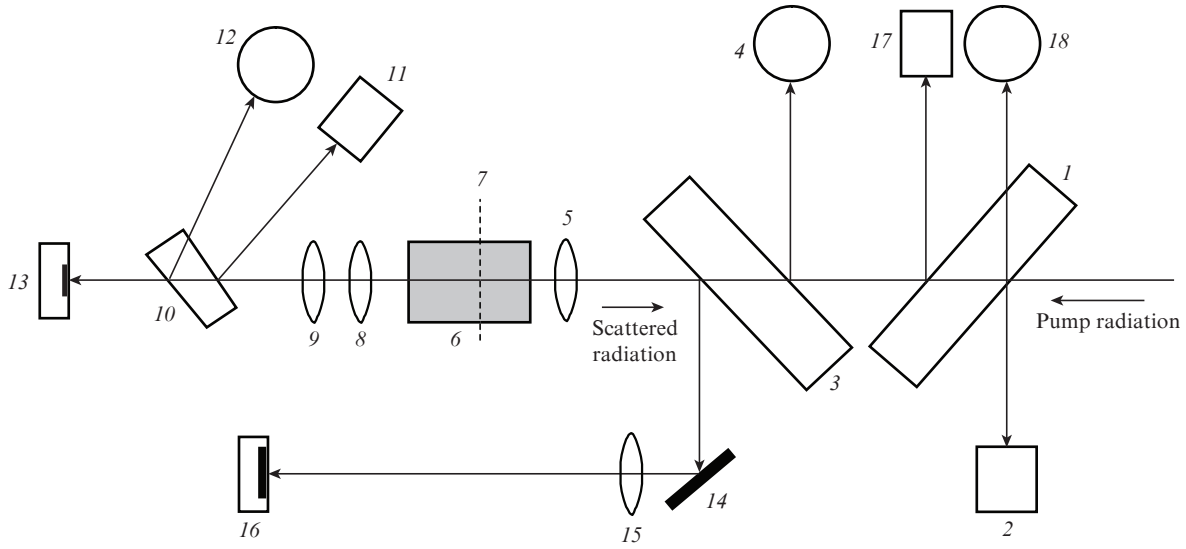

Figure 2. Schematic of the experimental setup: (*1*, *3*) plane-parallel glass plates; (*2*, *11*, *17*) calorimeters; (*4*, *12*, *18*) photodiodes; (*5*, *8*, *9*, *15*) lenses; (*6*) cell with toluene; (*7*) imaginary plane in the focus of lenses *5* and *8*; (*10*) glass wedge; (*13*, *16*) CCD matrices; (*14*) plane mirror.

of laser beams were recorded using WinCamD-USeries CCD matrices (UCM and UCD-12, DataRay corporation).

The pump beam was focused in a 7-cm-long toluene-filled cell (*6*) by lens *5* with a focal length $f = 3$ cm. Using lens *15* ($f = 160$ cm), the focal plane (*7*) of lens *5* was projected onto a CCD matrix (*16*) with a magnification of 53. The image obtained is a transverse spatial intensity distribution for the backscattered radiation (anti-Stokes STS component) emerging from the focal plane (*7*). In essence, this distribution characterises the divergence of anti-Stokes STS component. The image of the focal plane (*7*) in the pump beam passing through the cell (*6*) in the forward direction was projected [using lenses *8* ($f = 7$ cm) and *9* ($f = 75$ cm)] onto a CCD matrix (*13*) with a magnification of 10. The recorded image is a transverse spatial distribution of pump radiation intensity in the plane (*7*) within the active medium.

Figure 3 shows a series of images of transverse spatial intensity distributions for the backscattered anti-Stokes radiation and the pump radiation in the focal plane (*7*) of lens *5* (Fig. 2), recorded with increasing pump pulse energy. The top row contains spatial intensity distributions for the anti-Stokes STS component emerging from the focal plane (*7*), recorded by CCD matrix *16*. The bottom row contains spatial distributions of pump intensity in the plane (*7*), recorded by CCD matrix *13*. For each pair of the aforementioned, simultaneously recorded images, the energies of the pump pulse entering the cell (E_p^{in}), the anti-Stokes STS pulse (E_{STS}), and the pump pulse transmitted through the cell (E_p^{out}) were also measured. Using the measurement results for ten pulses, including the eight pulses depicted in Fig. 3 (see Table 1), we plotted (Fig. 4) a dependence of the fraction of pump pulse energy absorbed during wave interaction on the energy E_p^{in} of the pump pulse entering the cell:

$$\eta = \frac{E_p^{in} - (E_p^{out} + E_{STS})}{E_p^{in}},$$

The threshold pump pulse energy for STS excitation in our experimental conditions was ~1.3 mJ. For a linear process, the pump radiation with a divergence of 3×10^{-4} rad in the focus of lens with $f = 3$ cm (with allowance for the toluene refractive index $n \approx 1.5$) would form a focal spot with a diameter of ~14 μm. Then the pump radiation intensity in the focal plane of lens *5* (Fig. 2) would be 1.5×10^{10} W cm^{-2}. It follows from the data of Table 1 that the fraction of pump energy absorbed in toluene is ~40%. If all absorbed energy is released in the focal-waist region (where the main wave interaction occurs), the temperature of the latter should increase by $\Delta T = E_{abs}/(Cm)$, where E_{abs} is the absorbed energy, $C \approx 2$ J g^{-1} K^{-1} is the specific heat of toluene, and m is the toluene mass in this region. The toluene density is $\rho \approx 1$ g cm^{-3}, and the focal-waist volume is $V_f \approx 10^{-7}$ cm^3; therefore, the temperature will increase by $\Delta T = 5\times10^3$ K. For the time of laser pulse action, $\tau_{las} = 30$ ns, this region cannot be cooled via thermal conduction at toluene thermal diffusivity $\chi = 1.9\times10^{-3}$ cm^2 s^{-1}. Indeed, the heated region size is only $\sqrt{\chi\tau_{las}} \approx 7.5\times10^{-6}$ cm at a focal-waist diameter 1.4×10^{-3} cm.

Table 1.

Pulse number	E_p^{in}/mJ	E_p^{out}/mJ	E_{STS}/mJ
1	2.2	1.27	0.12
2	2.3	1.35	0.08
3	2.43	1.44	0.12
4	2.8	1.5	0.2
5	3.3	1.7	0.28
6	3.6	1.75	0.49
7	4.25	2.5	0.16
8	4.44	2.3	0.49

The following hypothesis was put forward to explain qualitatively the experimental results. Long before reaching the maximum temperature, a spatially inhomogeneous negative thermal lens is formed in the material because of heating. This leads to a rise in the pump beam diameter and, correspondingly, decreases its intensity. As a result, the two-photon absorption coefficient becomes so small that this process turns to be insignificant, and the wave interaction stops. Qualitatively, this process explains the pump-beam spatial transformation and limitation of the pump pulse energy transmitted through the cell.

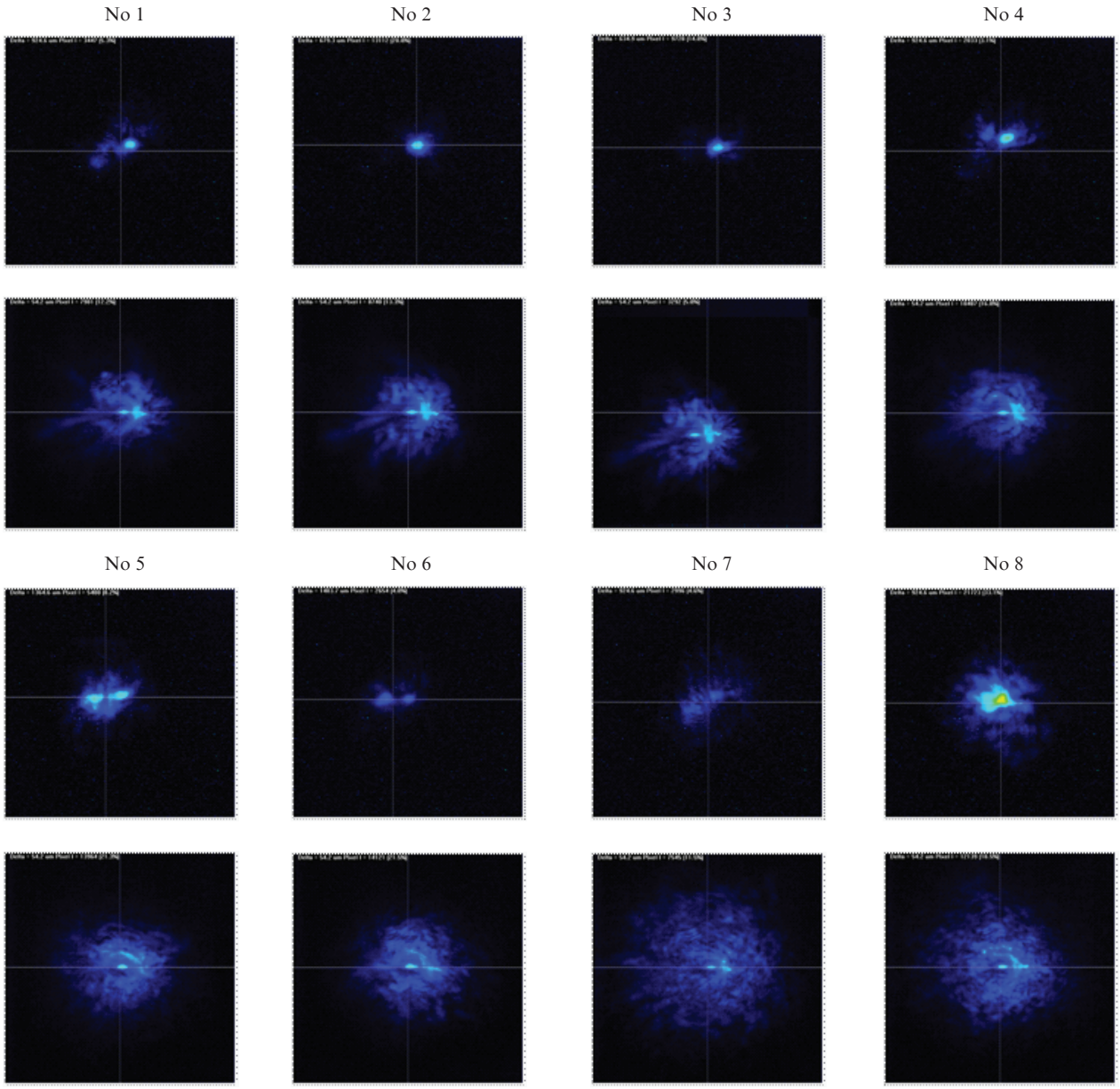

Figure 3. (Colour online) Transverse spatial distributions of radiation intensity for eight pulses recorded simultaneously by CCD matrices: (top row) anti-Stokes STS component (matrix *16*) and (bottom row) pump radiation transmitted through the cell (matrix *13*).

An analysis of photographs in Fig. 3 shows the following. Sometimes the focal distribution of anti-Stokes STS component intensity is comparable with the pump intensity distribution. This fact can be interpreted as phase conjugation at STS pump radiation. However, no less frequently these distributions have nothing in common. The same situation occurs for SBS when the pump beam is focused by a lens, because in this case sufficient discrimination of the spatial structure of spontaneous noises (with which the reflected radiation starts developing) is also absent. Concerning the spatial distribution of pump radiation intensity in the focal plane (*7*) of lens *5*, the situation observed here is different. The aforementioned distributions in each measurement have approximately the same structure: a narrow core with a wide spatially inhomogeneous background, although the background structure changes statistically from experiment to experiment. Another distortion of the spatial structure of passing radiation was observed in [2]; however, the authors related their result to low optical quality of the cell output window. In our case, this obviously does not hold true.

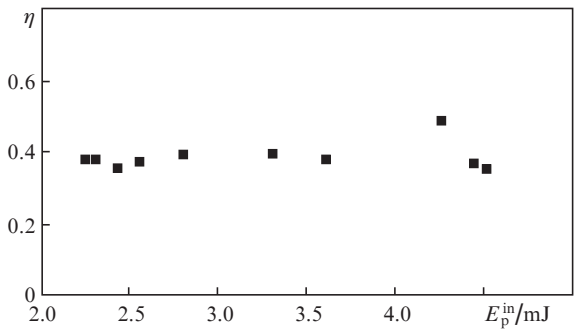

Figure 4. Dependence of the fraction of absorbed energy of a pump pulse on the pulse energy.

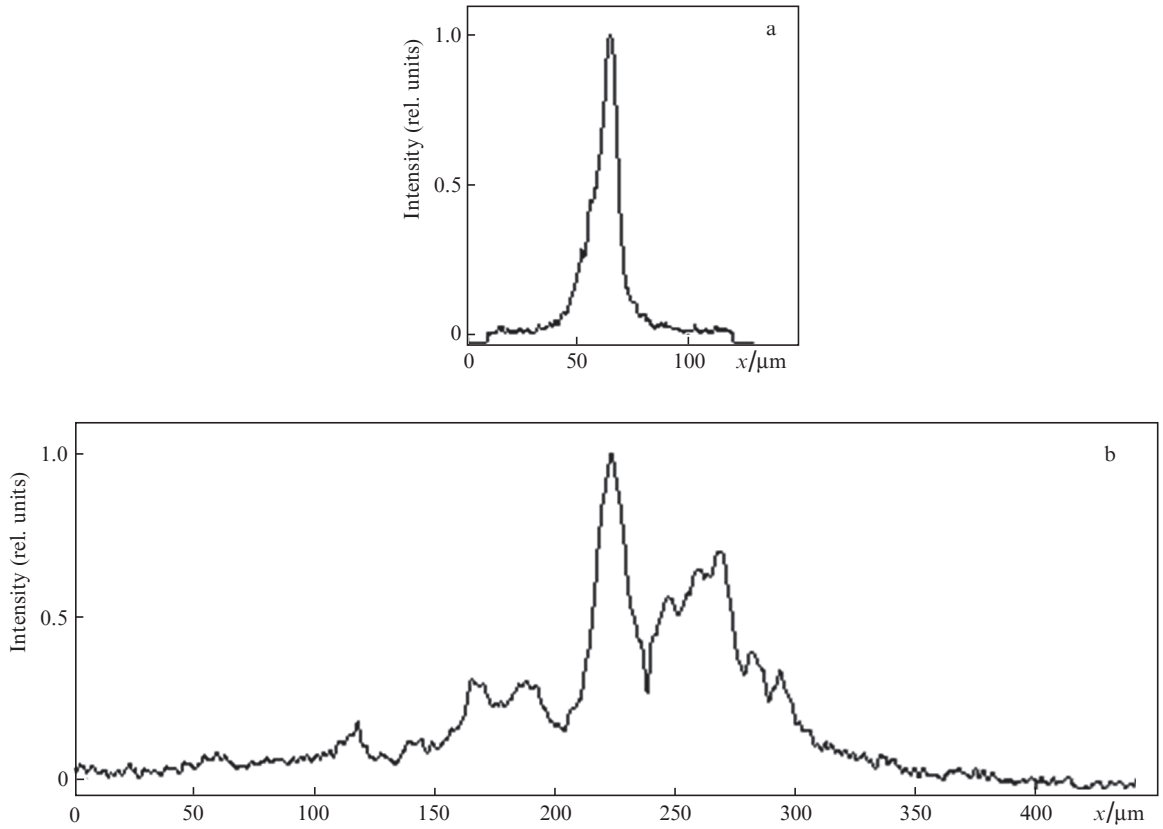

Figure 5. Normalised densitograms of radiation intensity (of the same scale) along the horizontal axis for frame No. 8 in Fig. 3: (a) anti-Stokes STS component and (b) pump radiation.

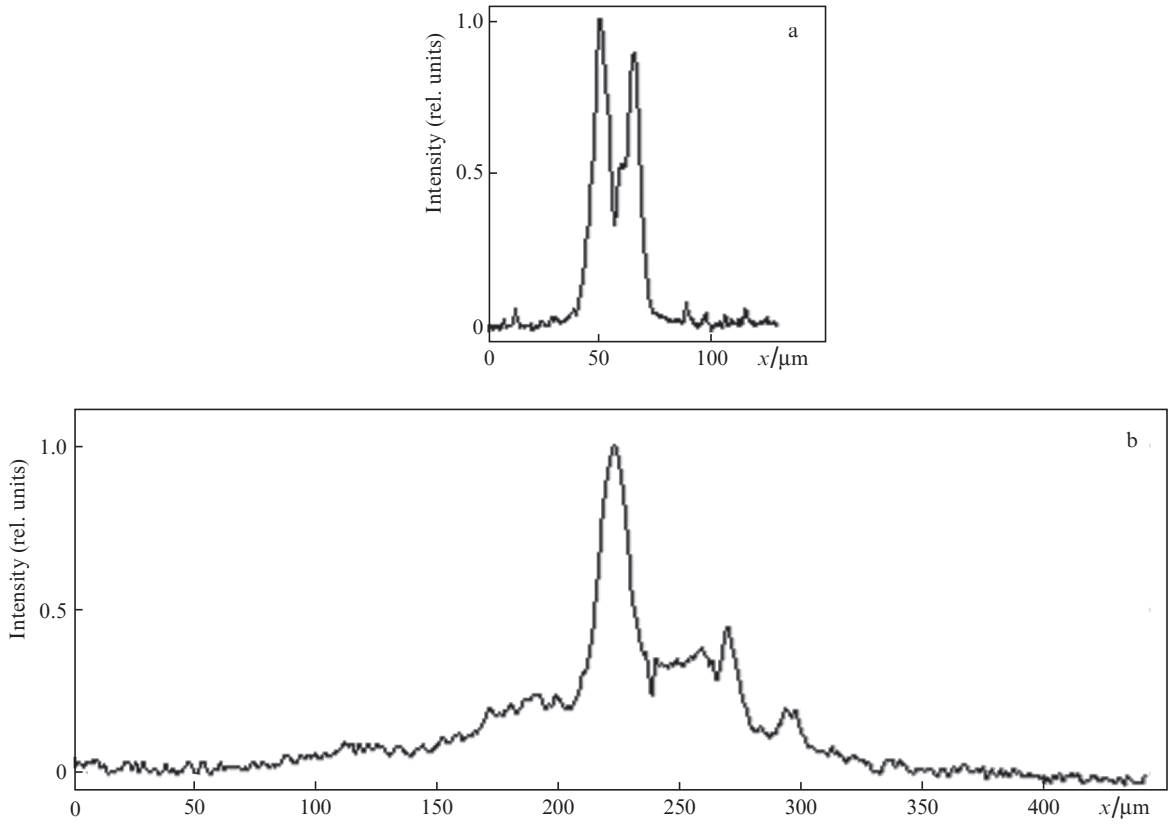

Figure 6. Normalised densitograms of radiation intensity (of the same scale) along the horizontal axis for frame No. 5 in Fig. 3: (a) anti-Stokes STS component and (b) pump radiation.

Based on the analysis of the photographs presented above (Fig. 3), it is natural to suggest that the anti-Stokes STS component is formed in the core region. The distribution of its intensity in the focal plane (*7*) (Fig. 2) does not coincide with the spatial structure of core in the pump intensity distribution in this plane. This conclusion is clearly demonstrated by the densitograms shown in Figs 5 and 6.

A processing of densitograms revealed that the core width at half maximum in Figs 5 and 6 is 20 and 16 μm, respectively. The half-width of the intensity distribution of the anti-Stokes STS component in Fig. 5 is 10 μm, whereas its intensity distribution in Fig. 6 consists of two peaks with half-widths of 8 and 9 μm, spaced by a distance of 16 μm. At the same time, the width of the intensity distribution for the background component of pump radiation is ∼400 μm and ∼300 μm in Figs 5 and 6, respectively. These values must be compared with the focal-waist diameter for pump radiation (14 μm in the linear case). Since the pump energy transmitted through the cell in Figs 5 and 6 is proportional to the area under the corresponding curves, it can be seen that the background-radiation energy exceeds that in the core. This, in our opinion, is caused by the disturbance of the optical properties of medium at two-photon absorption. Specifically this result we interpret as a decay of the spatial structure of pump radiation at STS due to its two-photon absorption in toluene. It should be emphasised that, since the two-photon absorption efficiency depends on the pump intensity, the radiation intensity distributions in the focal plane (*7*) (Fig. 2), measured by CCD matrices, are time-integrated. Here, it should be noted that the temperature of the finally formed focal-waist region with a diameter of ∼300 μm at the aforementioned values of absorbed pump energy (Fig. 4) is several tenths of kelvin.

Thus, the following facts were revealed experimentally: (i) a spatial decay of a pump beam in the focal-waist region at significant two-photon absorption of the neodymium-laser second harmonic in toluene and (ii) unusual (for stimulated-scattering processes) temporal behaviour of the pulses of the anti-Stokes STS component and pump radiation at the active medium output. The study should be continued to provide a more detailed interpretation of these experimental results.

References

1. He G.S., Yong K., Zhu J., Prasad P.N. *Phys. Rev. A*, **85**, 043839 (2012).
2. He G.S., Law W., Zhang X., Prasad P.N. *Appl. Phys. Lett.*, **101**, 011110 (2012).
3. He G.S., Law W., Baev A., Liu S., Swihart M.T., Prasad P.N. *J. Chem. Phys.*, **138**, 024202 (2013).
4. Shi I., Wu H., Yan F., Yang J., He X. *J. Nanopart. Res.*, **18**, 23 (2016).
5. Averyushkin A.S., Bulychev N.A., Efimkov V.F., Erokhin A.I., Kazaryan M.A., Mikhailov S.I., Saraeva I.N., Zubarev I.G. *Laser Phys.*, **27**, 055401 (2017).
6. Gordeev A.A., Efimkov V.F., Zubarev I.G., Mikhailov S.I. *Quantum Electron.*, **48** (9), 823 (2018) [*Kvantovaya Elektron.*, **48** (9), 823 (2018)].
7. Faris G.F., Gerken M., Jirauschek C., Hogan D., Chen Y. *Opt. Lett.*, **26** (23), 1894 (2001).